Journal of Power Sources 243 (2013) 617–621

Contents lists available at SciVerse ScienceDirect

Journal of Power Sources

journal homepage: www.elsevier.com/locate/jpowsour

Short communication

Optimized condition of high-frequency induction heating for $LiFePO_4$ with ideal crystal structure

Satoshi Uchida, Masaki Yamagata, Masashi Ishikawa*

Department of Chemistry and Materials Engineering, Faculty of Chemistry, Materials and Bioengineering, Kansai University, 3-3-35 Yamate-cho, Suita 564-8680, Osaka, Japan

HIGHLIGHTS

- Our original, high-frequency induction heating method for $LiFePO_4$/C synthesis is optimized.
- The key is a modified carbon crucible for effective precursor heating.
- Obtained $LiFePO_4$/C has ideal lattice parameters, theoretical capacity, and excellent rate capability.
- Such improved $LiFePO_4$/C is obtained by our technique only in 3 min.

ARTICLE INFO

Article history:
Received 27 May 2013
Accepted 9 June 2013
Available online 18 June 2013

Keywords:
Induction heating
Carbothermal reduction
$LiFePO_4$
Li-ion battery

ABSTRACT

The high-frequency induction heating method is an attractive way to synthesize $LiFePO_4$/C within a few minutes. We optimize the heating conditions by a carbon crucible for the homogeneous heating of a precursor pellet from both sides. Compared with our previous samples, the lattice parameters of the $LiFePO_4$/C synthesized in this work (an optimized sample) are improved and are much closer to the values reported by Padhi et al. Although the primary particle size of the optimized sample is slightly larger than that of the previous samples, it is sufficiently small to fully utilize the electrochemical performances of $LiFePO_4$. We reduced the internal charge-transfer resistance of the optimized sample by improving the crystal structure because the Nyquist plots of the electrodes indicate decreased resistance, even though the optimized sample's electronic conductivity is almost the same as that of the previous sample. The electrode based on the optimized sample shows a specific discharge capacity of 168.0 mAh g^{-1}, which achieves 99% theoretical specific capacity of the $LiFePO_4$ phase. Moreover, its charge–discharge rate performance is superior to that of the previous sample.

1. Introduction

All the consistent materials of Li-ion batteries must be improved and diversified to expand their use. Since most battery performances are dependent on the electrochemical properties of the electrode's active materials, the application of novel active materials to commercial Li-ion batteries is particularly crucial. Currently, $LiCoO_2$ is most widely used as a positive electrode material due to its high battery performances [1]; but cobalt is very expensive. Thus, there is a need for an inexpensive, high-performance positive electrode material instead of $LiCoO_2$ [2,3]. Lithium iron phosphate ($LiFePO_4$), which was reported by Padhi et al. [4], has a theoretical capacity of 170 mAh g^{-1} and relatively high redox potential around 3.5 V vs. Li/Li^+, which is attributed to an Fe^{2+}/Fe^{3+} redox couple. Furthermore, $LiFePO_4$ has better thermal stability and long-term cycle performance than $LiCoO_2$ [5]. The drawbacks of $LiFePO_4$ are low electronic conductivity derived from its lattice structure, including P—O covalent bonds [6] and poor Li-ion diffusion through a $LiFePO_4/FePO_4$ interface [4,7]. These problems have already been addressed by modifying the surface of $LiFePO_4$ particles with carbon [5,8] and by decreasing the particle size to nano-scale [9,10]. The $LiFePO_4$ modified with carbon ($LiFePO_4$/C) without the above drawbacks seems suitable as a positive electrode material for large-scale Li-ion batteries used in electric vehicles, plug-in hybrid electric vehicles, and large power storage systems. However, the market price of $LiFePO_4$/C is actually higher than $LiCoO_2$, even though it is produced from an inexpensive iron compound, thus limiting its wide practical application.

* Corresponding author.
E-mail address: masaishi@kansai-u.ac.jp (M. Ishikawa).

0378-7753/$ – see front matter © 2013 Elsevier B.V. All rights reserved.
http://dx.doi.org/10.1016/j.jpowsour.2013.06.051

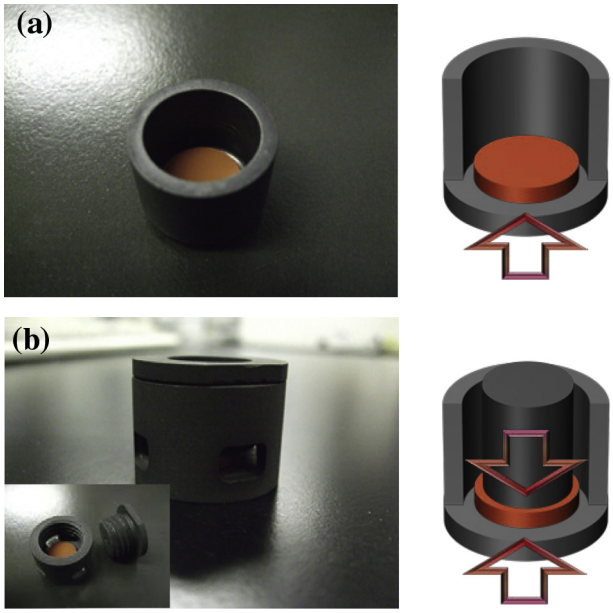

Fig. 1. Photographs and schematic images of carbon crucibles used in previous work (a) and this work (b).

$LiFePO_4$/C's high cost is mainly caused by the high temperature heating process in its synthesis procedure. Since the iron in the $LiFePO_4$ phase is divalent, the heating process must be carried out in an inert gas or a vacuum to suppress the oxidation of iron (from Fe^{2+} to Fe^{3+}) and long-time (typically several hours) heating is required [4–6]. In addition, using a divalent iron compound as an iron source, which enables easy synthesis of the $LiFePO_4$ phase, also increases $LiFePO_4$/C's cost. To synthesize $LiFePO_4$/C with superior electrochemical performances ascribed from its extremely small particle size and fine modification with carbon, various synthesis methods have been proposed in addition to typical solid-state reactions [4,6,11,12]. Such liquid phase synthesis methods as hydrothermal [13–15] and solvothermal methods [16–18] very effectively synthesize $LiFePO_4$/C with excellent battery performances. However, these methods are never completed only in a liquid phase process and eventually require a long-time heating process in an inert atmosphere or such a reductive gas flow as a mixed gas of H_2 with Ar. The spray pyrolysis method also requires an additional heating process in a reductive gas containing H_2 except for a pyrolysis process [19,20]. Since these methods increase the cost of $LiFePO_4$/C, we must use an inexpensive trivalent iron compound as an iron source and significantly reduce the heating time. Carbothermal reduction is necessary to use such a trivalent iron as Fe_2O_3. When a trivalent iron compound is heated with carbon or organic carbon sources at high temperature in an inert atmosphere, the trivalent iron compound is deprived of oxygen by carbon, and divalent irons are generated [21,22]. Previously reported microwave methods significantly reduce the heating time [23,24]. However, a microwave technique is difficult to control, and few reports have synthesized $LiFePO_4$/C with good battery performance [25,26].

Previously, we reported a novel rapid synthesis method for $LiFePO_4$/C [27] that combines a carbothermal reduction with a high-frequency induction heating method to reduce its material and process costs. In this method, a conductive crucible made of carbon or metal provides rapid heating (>1000 °C min^{-1}) by high-frequency induction, and the $LiFePO_4$ precursor is heated indirectly by the heat-radiating crucible. Our method is one solid-state reaction and can be easily controlled despite rapid synthesis in only a few minutes. The $LiFePO_4$/C synthesized in our method shows a maximum discharge capacity of 156 mAh g^{-1} at a 1/10 C-rate (1 C = 170 mA g^{-1}) and maintains 100.1 mAh g^{-1} even at a 10 C-rate. However, since the $LiFePO_4$ phase synthesized in our previous method did not have an ideal crystal structure, we decided to improve the pellet precursor, which was only heated from one side due to the shape of our carbon crucible (Fig. 1(a)); the heating time was also too short. In this work, we report the optimized heating condition using a crucible with an improved shape (Fig. 1(b)) for homogeneous heating of the pellet precursor from both sides. We compared the physical and electrochemical properties of the $LiFePO_4$/C synthesized in this work with those of a previous sample.

2. Experimental

The $LiFePO_4$/C sample was synthesized by a solid-state reaction of stoichiometric amounts of Li_2CO_3 (Kanto Chemical Co., 99.0%), Fe_2O_3 (Toda Kogyo Corp., 99.5%), and $NH_4H_2PO_4$ (Kanto Chemical Co., 99.0%) with citric acid (Kanto Chemical Co., 99.0%) as a carbon source. In this work, we increased the amount of citric acid to 12 wt.% (10 wt.% in the previous studies) because we anticipated a large citric acid loss due to the increased thermal conduction in the pellet precursor using a new carbon crucible where the pellet precursor was heated from both sides. The mixing process of the starting materials and the preparation process of the pellet precursor were identical to our previous work [27]. The pellet precursor was sandwiched between two parts of the carbon crucible for double-sided heating (Fig. 1(b)) and placed in a vacuum chamber. The carbon crucible was rapidly heated to 900 °C at 1800 °C min^{-1} by high-frequency induction heating and held for 1 min at maximum temperature. Since double-sided heating improved the reaction rate, the holding time at 900 °C was shortened more than in the previous work. After sintering at 900 °C, the temperature was reduced to 700 °C and held for 2 min for sufficient carbonization of the citric acid. We thoroughly ground the resulting grey pellet in a mortar and used the obtained powder as an active material.

X-ray diffraction (XRD, Rigaku Co., Ultima IV) with Cu Kα radiation was used to identify the phases of the synthesized samples. The diffraction data were collected in a step scanning mode under the same conditions as in previous work [27]. The carbon content of the synthesized samples was measured by X-ray fluorescence (XRF, Rigaku Co., ZSX Primus II) analysis, and the electric

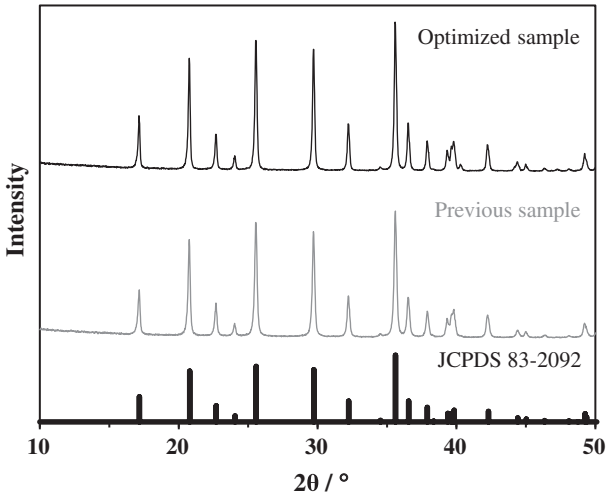

Fig. 2. XRD profiles of synthesized samples and reference pattern of $LiFePO_4$ (JCPDS 83-2092).

Table 1
Phase compositions obtained by Rietveld refinement and lattice parameters of $LiFePO_4$ phase calculated from XRD profiles.

Sample	Compositions (wt.%)		Lattice parameters (Å)		
	$LiFePO_4$	Fe_2P	*a*-axis	*b*-axis	*c*-axis
Previous sample	98.9	1.1	10.327	6.011	4.697
Optimized sample	100.0	0.0	10.335	6.008	4.695
Padhi et al. [4]	–	–	10.335	6.008	4.693

conductivity was measured by a four probe method. The obtained powder sample was pressed into a pellet at 5 MPa, and the four probes were pressed against the pellet. The measurement was performed ten times; the average value was regarded as representative electrical conductivity. We observed the morphology of the primary particles using a transmission electron microscope (TEM, JEOL Ltd., JEM-2100). The electron accelerating voltage was 120 kV. The primary particle-size distribution of the synthesized samples was determined by small-angle X-ray scattering (SAXS, Rigaku Co., Ultima IV). The measurement conditions of the scattering profiles were the same as in previous work [27]. The distribution was determined by curve fitting of the scattering profile with such parameters as background intensity, average particle size, normalized distribution ratio, scale factor, and the true density of $LiFePO_4$ (3.60 g cm^{-3}).

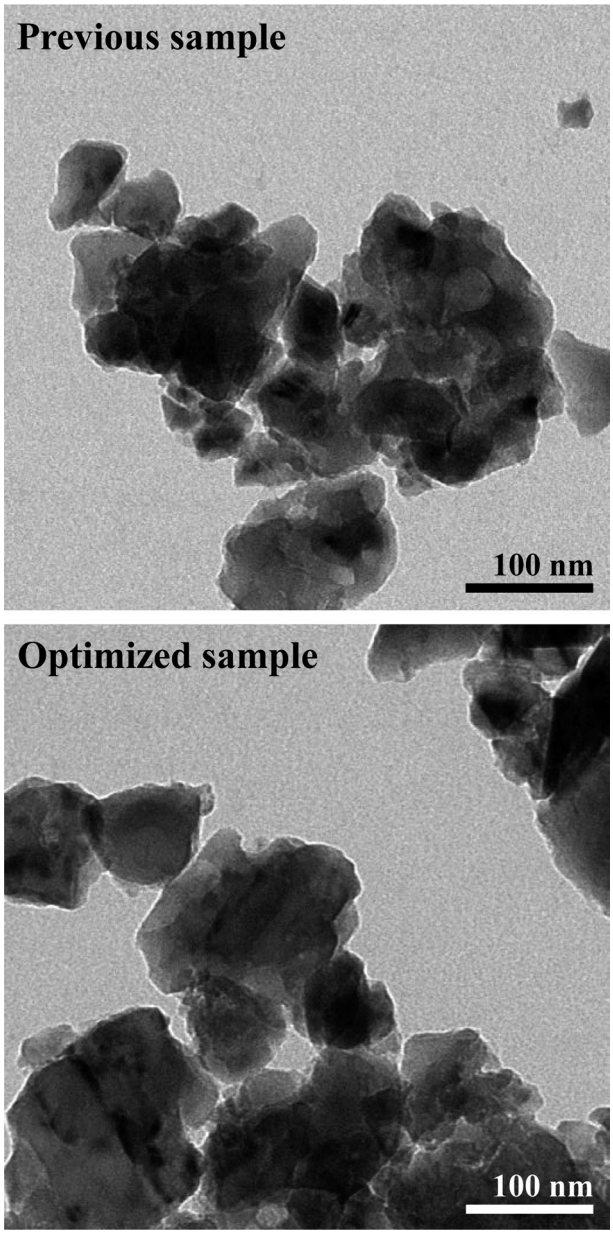

Fig. 3. TEM images of previous (a) and optimized (b) samples.

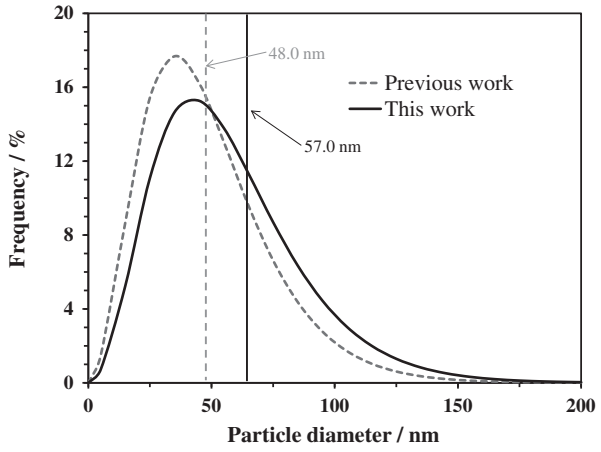

Fig. 4. Primary particle size distribution of previous (a) and optimized (b) samples.

We prepared positive electrodes for the electrochemical measurements from the obtained $LiFePO_4$/C, ketjen black (Lion Corp., Carbon ECP), and polyvinylidene fluoride (Kureha Corp., #1100) with respective weight ratios of 85:8:7 in the same way as in previous work [27]. The prepared positive electrode sheet was cut into 12-mm diameter disks as a test electrode. The mass loading of the active material to an electrode was approximately 6.0 mg cm^{-2}.

The electrochemical measurement was carried out using a CR2032 coin-type cell assembled in an argon-filled globe box. The composition of the positive-electrode half-cells was the same as in previous work [27]. The charge/discharge rate performance tests were carried out in a voltage range of 2.5–4.2 V using a galvanostatic charge/discharge unit (Intex Co., BTS2004W) at 1/10, 1/5, 1/2, 1, 3, 5, 10, and 20 C-rates (1 C = 170 mA g^{-1}) every five cycles. The charge and discharge cycle performance test was also carried out in the same voltage range at a 5 C-rate for 100 cycles following 5 pre-cycles at 1/10 and 1 C-rates. We measured the alternative current (AC) impedance spectra using a frequency response analyzer (Solartron analytical, 1255B). The measurement cell was charged to 80 mAh g^{-1} (approximate half-charging state) at a 1/10 C-rate after fully charging and discharging for 5 cycles at a 1/10 C-rate, and the cell voltage was relaxed for 10 h at an open-circuit condition for a steady-state impedance measurement. The measurement frequency range was 100 kHz–10 mHz.

3. Results and discussion

Fig. 2 shows the XRD profiles of the $LiFePO_4$/C synthesized in our previous work (previous sample) and this work (optimized sample). The reference pattern (JCPDS 83-2092) is displayed at the

Table 2
Average primary particle diameters and crystallite diameters obtained by Rietveld refinement of previous and optimized samples.

Sample	Average primary particle size	Crystallite diameter
Previous sample	48.0 nm	38.5 nm
Optimized sample	57.0 nm	48.0 nm

Table 3
Electronic conductivities and carbon contents of previous and optimized samples.

Sample	Electronic conductivity	Carbon content
Previous sample	1.9×10^{-2} S cm^{-1}	2.74 wt.%
Optimized sample	1.5×10^{-2} S cm^{-1}	2.26 wt.%

bottom. The crystalline impurities that can be confirmed by XRD are not included in the previous sample. On the other hand, the XRD profile of the optimized sample synthesized in a carbon crucible for heating the pellet precursor from both sides includes peaks attributed to the impurities. These peaks are related to a Fe_2P phase formed by over-reduction of the $LiFePO_4$ phase. The Fe_2P content in the optimized sample, which is obtained by Rietveld refinement, is 1.1 wt.% (Table 1). Fe_2P improves the conductivity of $LiFePO_4$ without affecting the cycle stability [28]. A large amount of Fe_2P formation decreased the $LiFePO_4$ phase in the sample, which decreased the maximum specific capacity, but the presence of a small amount of Fe_2P is not a crucial problem [28]. The lattice parameters of the $LiFePO_4$ phase calculated from each XRD profile are shown in Table 1. The lattice parameter is an important factor that significantly affects the electrochemical properties of the $LiFePO_4$ phase [29]. The lattice parameters of the previous sample deviate from the values reported by Padhi et al. We believe that this deviation was caused by asymmetrically heating only one side of the pellet precursor. Thus, we improved the configuration of the carbon crucible to achieve homogeneous heating. The optimized sample synthesized by the modified carbon crucible for heating the pellet precursor from both sides has ideal lattice parameters that are close to those reported by Padhi et al. Note that the $LiFePO_4$ phase with ideal crystal structure was successfully generated despite such a short heating time as 3 min.

Figs. 3 and 4 show the TEM images and the primary particle distributions of the synthesized samples. The $LiFePO_4$/C synthesized by our method is essentially a composite of $LiFePO_4$ and carbon. The primary particle size confirmed by the TEM images is 50–150 nm; the optimized sample particles seem slightly larger. The particle size growth was probably promoted since thermal conduction to the pellet precursor is enhanced by the modified carbon crucible. The primary particle size distribution of the optimized sample is slightly larger than the previous sample in Fig. 4, which is consistent with the TEM observation results. The average primary particle size and the crystallite diameter of both samples are listed in Table 2. The crystallite diameter and the average primary particle size are essentially similar in each sample, indicating

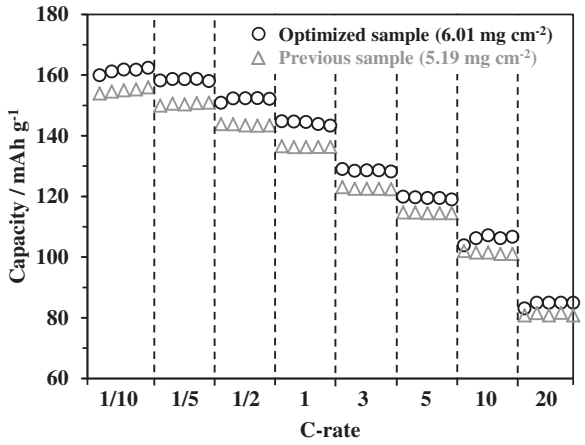

Fig. 6. Discharge capacity vs. charge and discharge rates of positive electrodes based on previous and optimized samples.

that a primary particle is a single crystal or is composed of a few crystallites. Although the difference in the heating conditions leads to slight differences in the particle size, both samples retain their small particle size and are expected to fully exhibit the electrochemical performances of $LiFePO_4$.

Table 3 lists the electronic conductivities obtained by the four-probe measurement and the carbon content measured by the XRF of both samples. The electronic conductivity of the optimized sample is almost identical to that of the previous sample, even though the optimized sample's carbon content is less than that of the previous sample. Since the optimized sample includes small amounts of Fe_2P (Table 1), which is a conductive impurity, its electronic conductivity is equivalent to the previous sample despite less carbon content.

Fig. 5 shows the charge and discharge curves at 1/10, 1, and 5 C-rates of the positive electrodes based on the previous and optimized samples. At the 1/10 C-rate, the positive electrode with the previous sample shows a discharge capacity of 156.0 mAh g^{-1}, which has not reached a theoretical capacity. On the other hand, the positive electrode based on the modified sample shows a discharge capacity of 162.4 mAh g^{-1}. This specific capacity is normalized by the weight including the carbon and the Fe_2P, but the specific capacity normalized by the weight of only $LiFePO_4$ corresponds to 168.0 mAh g^{-1}, which is 99% of the theoretical capacity. Furthermore, the optimized sample has a longer voltage plateau region that indicates a well-defined two-phase ($LiFePO_4$/$FePO_4$)

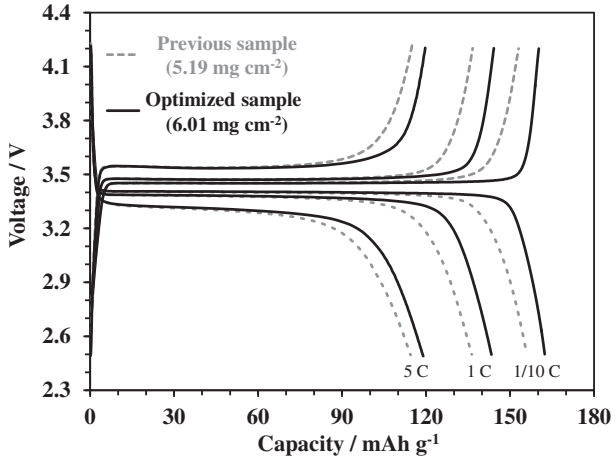

Fig. 5. Charge and discharge curves at various C-rates of positive electrodes prepared from previous and optimized samples.

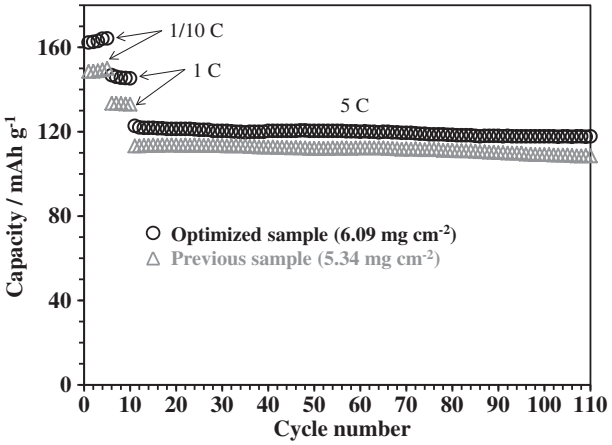

Fig. 7. Discharge capacity vs. cycle number of positive electrodes based on previous and optimized samples.

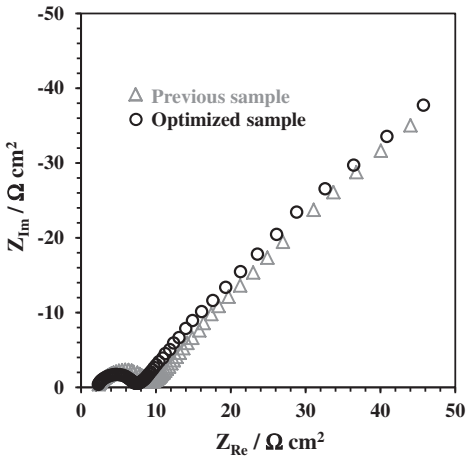

Fig. 8. Nyquist plots of positive electrodes based on previous and optimized samples, measured at half-charging state (80 mAh g^{-1}) at 6th cycle.

coexistence reaction [7]; such an ideal two-phase reaction is also supported by the sharp rise and drop in the charge and discharge curves. Fig. 6 shows the discharge capacity vs. the charge and discharge rates of the positive electrode containing the previous and optimized samples. The positive electrode based on the optimized sample shows higher capacity than the positive electrode prepared from the previous sample at all 1/10–20 C-rates. Although mass loading of the optimized sample to the electrode is somewhat higher than the previous one, the optimized sample's rate performance is clearly improved. Fig. 7 shows the discharge capacity vs. the cycle number at a 5 C-rate after initial lower rate cycles. The capacity of the positive electrode prepared from the previous sample appears to degrade slightly at 110 cycles. The voltage plateau of $LiFePO_4$ is at about 3.5 V (Fig. 5), where no electrolyte decomposition occurs, and at the present high rate of 5 C, there is a negligible period when the electrode potential exceeds 3.8 V where an electrolyte might decompose. Therefore, the capacity degradation in this cycle test can probably be attributed to the deterioration of $LiFePO_4$. The positive electrode prepared from the optimized sample exhibits almost no capacity degradation. The $LiFePO_4$ phase with ideal crystal structure improves the cycle stability.

Fig. 8 shows the Nyquist plots of the positive electrodes containing the previous and optimized samples. The mass loading of the active material to each electrode for the AC impedance measurement is approximately the same. We carried out the measurement at an equilibrium state after the cell voltage was adequately relaxed, and the Nyquist plots of the cells show only one semicircle and a straight line with a 45° slope. The semicircle contains both the internal charge-transfer resistance of the electrode active material and the charge-transfer resistance through the electrode/electrolyte interface. The electronic conductivity of the optimized sample is almost the same (or slightly less) as the previous sample (Table 3), and its mean particle diameter increases (Fig. 3 and Table 2); in other words, its active surface area decreases. These tendencies are likely to increase the semicircle of the AC response of the optimized sample. In fact, however, it becomes rather smaller than the previous sample. Therefore, we believe that the internal charge-transfer resistance of the optimized sample decreases as its crystal structure is improved.

4. Conclusions

We optimized the heating condition of the high-frequency induction heating method for $LiFePO_4$/C synthesis by a modified carbon crucible to homogeneously heat the pellet precursor from both sides. We successfully obtained optimized $LiFePO_4$/C with ideal lattice parameters close to the values reported by Padhi et al. Although the optimized sample has a slightly larger primary particle size and slightly lower electronic conductivity than the previous sample, the semicircle size in the Nyquist plot of the electrode containing the optimized sample is smaller than that of the previous sample. The electrode based on the optimized sample shows a specific discharge capacity of 168.0 mAh g^{-1}, which achieves 99% of the theoretical specific capacity of the $LiFePO_4$ phase. The charge and discharge rate performance of the optimized electrode is superior to that of the previous electrode in the range of the 1/10–20 C-rates. The optimized electrode also shows excellent cycle stability during 100 cycles at the 5 C-rate. These improved results are attributed to the ideal crystal structure of the $LiFePO_4$ phase obtained by the homogeneous heating condition. This study clearly shows that $LiFePO_4$/C with an ideal crystal structure and excellent electrochemical performances can be synthesized in an extremely short time (ca. 3 min) by homogeneous, high-frequency induction heating and will significantly reduce its cost.

Acknowledgements

The carbon content analysis using XRF in this work was carried out by the Rigaku Corporation. This work was partly supported by the "Strategic Project to Support the Formation of Research Bases at Private Universities", which is a Matching Fund Subsidy from the Ministry of Education, Culture, Sports, Science and Technology (MEXT), 2009–2014.

References

[1] T. Ohzuku, A. Ueda, J. Electrochem. Soc. 141 (1994) 2972.
[2] T. Ohzuku, Y. Makimura, Chem. Lett. 2001 (2001) 744.
[3] T. Ohzuku, Y. Makimura, Chem. Lett. 2001 (2001) 642.
[4] A.K. Padhi, K.S. Nanjundaswamy, J.B. Goodenough, J. Electrochem. Soc. 144 (1997) 1188.
[5] H. Huang, S.-C. Yin, L.F. Nazar, Electrochem. Solid-State Lett. 4 (2001) A170.
[6] A. Yamada, S.C. Chung, K. Hinokuma, J. Electrochem. Soc. 148 (2001) A224.
[7] L. Laffont, C. Delacourt, P. Gibot, M.Y. Wu, P. Kooyman, C. Masquelier, J.M. Tarascon, Chem. Mater. 18 (2006) 5520.
[8] Z. Chen, J.R. Dahn, J. Electrochem. Soc. 149 (2002) A1184.
[9] C. Delacourt, P. Poizot, S. Levasseur, C. Masquelier, Electrochem. Solid-State Lett. 9 (2006) A352.
[10] K.F. Hsu, S.Y. Tsay, B.J. Hwang, J. Mater. Chem. 14 (2004) 2690.
[11] M.M. Doeff, Y. Hu, F. McLarnon, R. Kostecki, Electrochem. Solid-State Lett. 6 (2003) A207.
[12] F. Croce, A. D'Epifanio, J. Hassoun, A. Deptula, T. Olczac, B. Scrosati, Electrochem. Solid-State Lett. 5 (2002) A47.
[13] X. Ou, H. Gu, Y. Wu, J. Lu, Y. Zheng, Electrochim. Acta 96 (2013) 230.
[14] J. Ni, M. Morishita, Y. Kawabe, M. Watada, N. Takeichi, T. Sakai, J. Power Sources 195 (2010) 2877.
[15] A. Kuwahara, S. Suzuki, M. Miyayama, Ceram. Int. 34 (2008) 863.
[16] Q. Wang, W. Zhang, Z. Yang, S. Weng, Z. Jin, J. Power Sources 196 (2011) 10176.
[17] H. Deng, S. Jin, L. Zhan, W. Qiao, L. Ling, Electrochim. Acta 78 (2012) 633.
[18] S. Yang, X. Zhou, J. Zhang, Z. Liu, J. Mater. Chem. 20 (2010) 8086.
[19] M. Konarova, I. Taniguchi, J. Power Sources 195 (2010) 3661.
[20] N.A. Hamid, S. Wennig, S. Hardt, A. Heinzel, C. Schulz, H. Wiggers, J. Power Sources 216 (2012) 76.
[21] J. Barker, M.Y. Saidi, J.L. Swoyer, Electrochem. Solid-State Lett. 6 (2003) A53.
[22] H.P. Liu, Z.X. Wang, X.H. Li, H.J. Guo, W.J. Peng, Y.H. Zhang, Q.Y. Hu, J. Power Sources 184 (2008) 469.
[23] Y. Zhang, H. Feng, X. Wu, L. Wang, A. Zhang, T. Xia, H. Dong, M. Liu, Electrochim. Acta 54 (2009) 3206.
[24] M. Higuchi, K. Katayama, Y. Azuma, M. Yukawa, M. Suhara, J. Power Sources 119 (2003) 258.
[25] M.S. Song, D.Y. Kim, Y.M. Kang, Y.I. Kim, J.Y. Lee, H.S. Kwon, J. Power Sources 180 (2008) 546.
[26] M.S. Song, Y.M. Kang, J.H. Kim, H.S. Kim, D.Y. Kim, H.S. Kwon, J.Y. Lee, J. Power Sources 166 (2007) 260.
[27] S. Uchida, M. Yamagata, M. Ishikawa, Electrochemistry 80 (2012) 825.
[28] C.W. Kim, J.S. Park, K.S. Lee, J. Power Sources 163 (2006) 144.
[29] J.F. Martin, A. Yamada, G. Kobayashi, S. Nishimura, R. Kanno, D. Guyomard, N. Dupré, Electrochem. Solid-State Lett. 11 (2008) A12.